PERGAMON

International Journal of Heat and Mass Transfer 41 (1998) 3937–3948

International Journal of HEAT and MASS TRANSFER

Classification of one-dimensional steady-state two-phase geothermal flows including permeability variations—II. The general case

R. M. Young*

N.Z. Institute for Industrial Research and Development, P.O. Box 31-310, Lower Hutt, New Zealand

Received 8 August 1996; in final form 12 February 1998

Abstract

In Part II of this paper the analysis is extended to include both conduction and non-zero net mass flow. We are able to distinguish between low and high enthalpy two-phase reservoirs, where the former must terminate in single-phase liquid conditions at depth, while the latter may end in single-phase liquid (for low permeabilities), single-phase vapour (for intermediate permeabilities), or can be unstable when extended (for high permeabilities). If, and only if, both conduction and net mass flow are non-zero a class of models can be identified with the property that a permeability increase (downwards) is associated with a liquid saturation decrease. This provides a prototype for a vapour-dominated geothermal reservoir.

1. Introduction

In Part I of this paper [1] we used the flowplane diagram method to study some special cases of one-dimensional steady-state two-phase geothermal flows. The method can be used to construct idealized models of heterogeneous two-phase geothermal reservoirs in the natural state. In particular, we isolated the influences of conduction and net mass flow in examples of (a) the heatpipe (zero net mass flow), and (b) purely convective flow (zero conduction).

In Part II we continue the analysis by extending the flowplane diagram to the general case where there is both non-zero net mass flow and conduction. The signatures of the individual physical mechanisms (conduction, net mass flow) can still be identified in the diagram, but we shall show that there is an important additional effect which occurs when they interact. As in [1] the classification process is essentially geometrical, and we are usually able to establish a close connection between the geometry and the physics. The major structures are the pressure trajectories which represent the pressure and saturation profiles in a homogeneous vertical two-phase column, and the pressure contours which can be used to track the flow through permeability contrasts.

Vapour-dominated reservoirs. This study also has relevance to a particular difficulty referred to in the conclusion to [1]: in all cases studied the flowplane geometry was such that a permeability increase (downwards) was necessarily accompanied by a rise in liquid content. This result is in conflict with a commonly held view (see for example [2, 3]) that vapour-dominated conditions develop in the natural state of some geothermal reservoirs due to the presence of a low permeability structure (the caprock) separating the geothermal aquifer from the groundwater aquifer. According to this hypothesis (described by Straus and Schubert in [3]) the sudden permeability increase across the caprock/geothermal-aquifer boundary induces vapour-dominated conditions in the aquifer. In contrast, the theory developed in [1] predicts that the saturation change at such a boundary would be in the opposite direction, generally leading to liquid-dominated conditions within the aquifer. However the numerical simulation experiments of Ingebritsen and Sorey [4] demonstrate that the caprock hypothesis is well-founded, and that vapour-dominated reservoirs do in fact develop under these conditions. Furthermore, the

* Corresponding author. Tel.: 00 64 4 5690247; fax: 00 64 4 569003; e-mail: roger@maths.grace.cri.nz

0017–9310/98 $19.00
PII: S0017–9310(98)00090–8

existence of vapour-dominated geothermal reservoirs (The Geysers, Yellowstone National Park; Kawah Kamojang, Indonesia, etc.) is an established fact. The problem then is to reconcile the theoretical predictions of the one-dimensional model with numerical experiment and observation.

One possible explanation for the apparent failure of the one-dimensional theory to predict the existence of vapour-dominated (VD) reservoirs is that VD reservoirs are genuinely multi-dimensional phenomena, just like convection cells in single-phase reservoirs. This hypothesis gains plausibility from some recent work [5, 6] which shows that the one-dimensional steady-state VD reservoir model of Kawah Kamojang proposed by Straus and Schubert in [3] is, in fact, unstable. Furthermore, Ingebritsen and Sorey's simulation of a VD reservoir was two-dimensional.

Although there may be some merit in the multi-dimensional hypothesis, we shall show in this paper that there is a simple alternative model of a VD reservoir which is both one-dimensional and stable. It can be explained in terms of the general flowplane diagram described below.

Assumptions. The restrictions on the model discussed in [1] are again made here (we assume the reader's familiarity with this paper), namely we are concerned with steady-state one-dimensional porous media flow containing a two-phase steam/water leg. A normalization condition is imposed on the relative permeability functions [1]. Capillarity is not explicitly included in our formulation, but the macroscopic effects of capillarity are fully-accounted for in the flowplane diagram [1]. Steady-state flow is maintained by means of geothermal boundary conditions, by which is meant the imposition of a Dirichlet boundary condition at ground surface (prescribed pressure and temperature) and a Neumann, or flow, boundary condition at depth (fixed mass and energy flows).

Plan of this paper. We preface the main body of the paper with an example of a simulated one-dimensional steady-state flow. Computed saturation-depth profiles are presented for a reservoir containing a single fixed-magnitude permeability discontinuity. In the next section the major features of the general flowplane diagram are summarized, and a geometrical classification is introduced which distinguishes between certain physically different reservoir models. The case of a high enthalpy reservoir is discussed. The flowplane method is then applied to the simulation example of the previous section. Finally we describe a prototype one-dimensional model for a vapour-dominated geothermal reservoir. Some results from a two-dimensional simulation of a VD reservoir [4] are compared with the proposed one-dimensional model.

Notation. We shall freely refer to sections, equations, figures and tables in Part I of this paper [1]. We shall distinguish these references with a superscript *. Thus, equation (5*) refers to equation (5) of [1], etc.

2. Saturation profiles with a permeability discontinuity

A rapid permeability change may be approximated as a permeability discontinuity. The presence of a permeability contrast will change the geothermal steady state, and in two-phase conditions a permeability discontinuity will be accompanied by a step change in saturation. We present some results from a numerical simulation of one-dimensional flow.

Figure 1 shows a sequence of steady-state (liquid) saturation profiles for a model containing a permeability discontinuity (dotted line). In the figure gravity acts to the right and the horizontal dashed lines are the residual saturations. All the examples have the same steady-state mass and energy flows ($J_M = -10^{-6}$ kg s^{-1} m^{-2}, $J_E = -2.9$ W m^{-2}), the same constant conductivity ($K = 4$ W m^{-1} K^{-1}) and the same permeability contrast between high (H) ($k = 4$ md $= 4 \times 10^{-15}$ m^2) and low (L) ($k = 0.04$ md $= 4 \times 10^{-17}$ m^2) permeabilities. These mass and energy flows (and conductivity) are similar to values chosen in [3] to model the Kawah Kamojang reservoir. The upper surface boundary condition (the same in all cases) is $P_0 = 10^5$ Pa and $T_0 = 15^\circ$C. The distinguishing feature in the various cases is thus the location of the permeability discontinuity.

Figure 1 is based on numerical results using the TOUGH2 geothermal simulator [7]. A vertical section of depth 1200 m within a geothermal reservoir has been approximated as a one-dimensional column. Starting from an initial single-phase state of constant pressure and temperature the boundary conditions are applied at top ($P = P_0, T = T_0$) and bottom (J_M, J_E), and the system is run to steady-state. In all cases a phase boundary appears, separating an upper single-phase liquid zone from an underlying two-phase region. The location of this interface is determined by the upper boundary condition [8] and the permeability distribution; note that it is generally not coincident with the permeability discontinuity. The saturation jump at the interface consists of two parts: a jump through the immobile steam saturations which are always excluded in the steady-state [9]; and an additional jump to a saturation for which both phases are mobile. Piecewise linear relative permeability functions have been employed in the simulation with residual saturations $S_{rw} = 0.1 = S_{rs}$; but note that all the results in this paper are independent of the choice of relative permeability function satisfying the normality condition, equation (1*). As a partial check on some results the simulations have been run both without and with capillarity (using Leverett's J-function). The results are essentially identical. This confirms that our formulation of the steady-state problem represents the macroscopic effects of capillarity correctly.

In Fig. 1(i) the permeability discontinuity is high up in the single-phase liquid region. A liquid-dominated two-phase zone develops beneath the phase boundary with

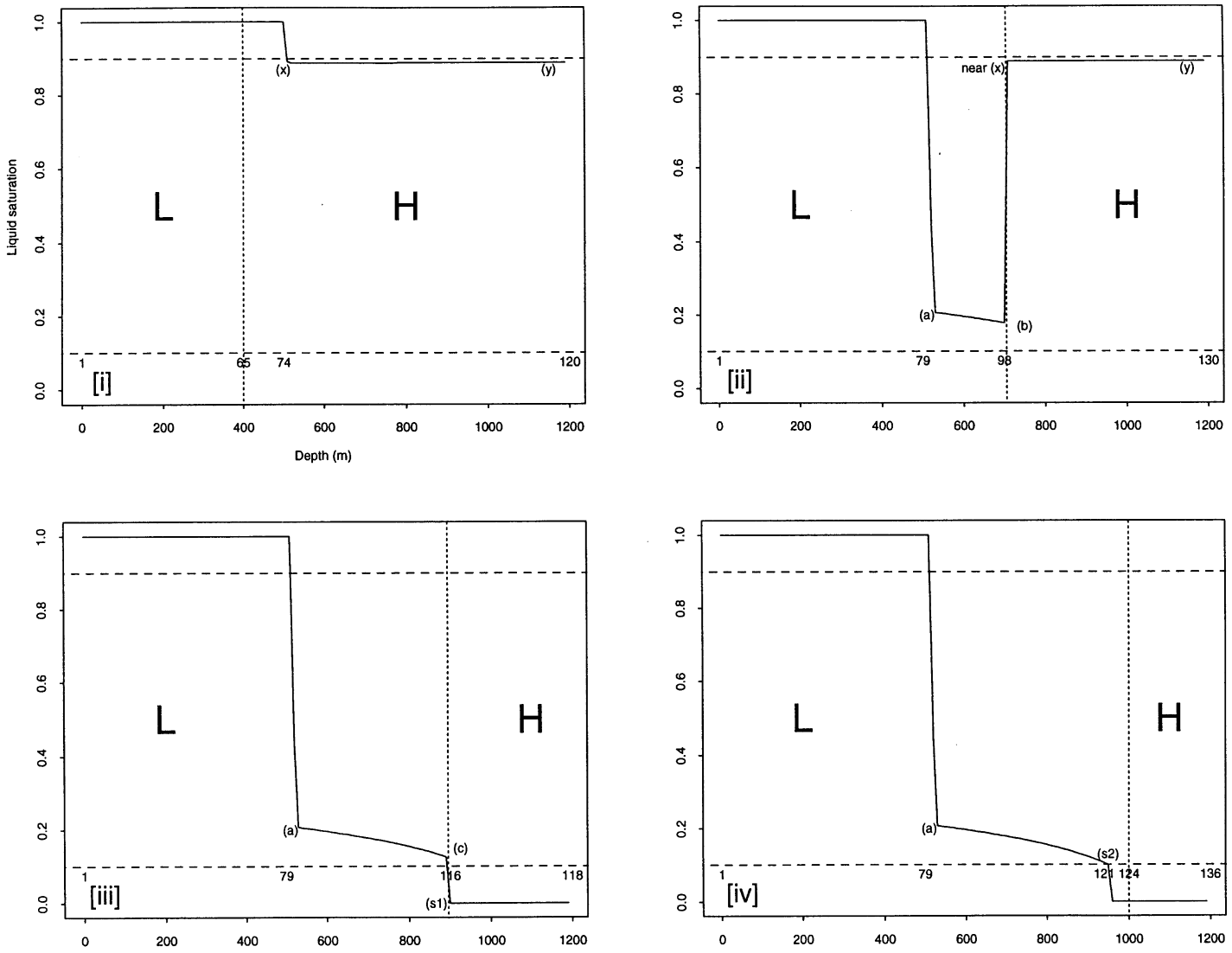

Fig. 1. Saturation–depth profiles for a 1200 m vertical column (gravity acts to the right) containing a permeability discontinuity (denoted by the vertical dotted line) at various depths. The discontinuity separates low (L) and high (H) permeabilities. The dashed horizontal lines are the residual saturations. Numbers near the bottom of each diagram are the pressures (in bars) at the indicated depths. Symbols in parentheses refer to Fig. 2(iii).

the saturation gradually decreasing with depth. In Fig. 1(ii) the discontinuity occurs below the phase boundary: the two-phase zone is initially vapour-dominated with gradually decreasing liquid saturation as far as the discontinuity, then a saturation jump to liquid-dominated conditions occurs followed by a second gradual decrease as in (i). In Fig. 1(iii) the permeability discontinuity is only 200 m below that in the previous example, but the second saturation discontinuity is now in the opposite direction. Below the permeability-controlled saturation discontinuity is a region of single-phase vapour. Case (iv) is similar to Case (iii) except that the permeability discontinuity is now below the two-phase region. Thus, the second saturation discontinuity is no longer defined by the permeability contrast, instead the two-phase zone is terminated when the saturation reaches the liquid residual value.

Some features of Fig. 1 have already been encountered in Part 1 of this paper [1]. The upper phase transition in all cases may be identified as type (WT) (see Table 1*), and, since the saturation wavespeed $C < 0$, this is a jump transition, from $S = 1$ (single-phase liquid) to some value $S < S^*$ where $S_{rs} = 1 - S^*$ is the vapour-residual value. This is observed in Fig. 1: note the magnitude of the jump $S^* - S$ is much greater in the low permeability cases. Secondly, Table 1* predicts that the transition at the lower phase boundary of type (TS) or (TW) must be smooth from two-phase to single-phase. When immobile liquid or vapour is present this is interpreted to mean that the saturation must tend smoothly towards the appropriate residual value. This is observed in Fig. 1(iv). In Figs 1(i) and (ii) the two-phase zone does not terminate so the issue is undecided. Figure 1(ii) shows an example of a permeability-controlled saturation jump: a permeability increase (downwards) is associated with a liquid saturation increase, similar to Fig. 3*(ii) in [1].

In spite of the agreement of some aspects of Fig. 1 with previous results (1), the third diagram Fig. 1(iii) is quite anomalous. The permeability-controlled saturation jump in (iii) is the opposite direction to that of (ii), even though the permeability discontinuities are only 200 m apart. In (ii) a permeability increase induces a saturation increase, but in (iii) just the opposite happens. These points will be re-examined later in this paper. At this stage we remark that caprock hypothesis [3] on vapour-dominated reservoirs seems to be supported by Fig. 1(iii), but not by Fig. 1(ii).

3. The flowplane diagram: the general case

Description. The flowplane diagram is a simple and informative technique for representing the major features of one-dimensional two-phase flow in a heterogeneous formation. Physical mechanisms such as conduction and net mass throughflow have a particular geometrical signature in the flowplane. The saturation associated with a given flowstate is obtained by means of a simple geometric construction. The flowplane diagram is discussed fully in references [1, 6, 10]. In particular we assume the reader is familiar with the presentation given in Part I of this paper [1].

Permeability contrasts. The zero net mass flow and no-conduction examples presented in [1] all have one characteristic in common: the flowplane pressure contours are straight lines passing through the flowplane origin (in both cases the interaction term i is zero). Without exception this implies that a positive permeability contrast (permeability increase with depth) induces an increase in liquid saturation.

Now although this result seems intuitively reasonable, it conflicts with the caprock hypothesis proposed by Straus and Schubert [3] for vapour-dominated reservoirs. According to this hypothesis vapour-dominated conditions are first established in a zone of low permeability L ('cap rock'); vapour-dominated conditions are then also propagated (somehow) to the high permeability aquifer H which underlies L. Ingebritsen and Sorey [4] gave some plausibility to the Straus/Schubert proposal by constructing a two-dimensional simulation model of a reservoir bounded by a low permeability aureole. They found in their examples that vapour-dominated conditions developed in the reservoir provided the caprock permeability was sufficiently small and the reservoir permeability was sufficiently large.

However, according to the theorem established in [1], a permeability increase (downward) will tend to augment the liquid saturation, and if the increase is of the order of one or two magnitudes then vapour-dominated conditions in the caprock will be replaced by liquid-dominated conditions in the aquifer. This is precisely the situation demonstrated in Fig. 1(ii).

In this section we will resolve the apparent contradiction. We will show that conduction is the missing ingredient in the specimen examples considered so far (or, more precisely, the non-zero product of conductivity with the net mass flow), and that the flowplane diagram gives a convincing explanation of its vital role in the formation of vapour-dominated geothermal reservoirs. The general form of the flowplane diagram exhibits all the complexities of the various special cases, as well as additional complications. We shall not attempt to give a comprehensive description of the general case, but rather concentrate on the salient features.

3.1. *Classification*

We now use the geometrical properties of the flowplane trajectories as a basis for the classification of one-dimensional steady-state two-phase flows. It turns out that the thermodynamics of the fluid at the critical point enters heavily into this classification. However it should be

emphasized that this does not mean that the actual fluid state need be anywhere near critical. In fact, by definition, two-phase states are always below critical.

Following the method in [1] we begin by examining the behaviour of the flowplane trajectories as the pressure approaches the critical value ($P_c = 221.2$ bars). It follows from equation (9*) that as $P \to P_c$ the pressure trajectories approach infinity in the quadrants Q_2 or Q_4 according as

$$(J_E - h_c J_M + \gamma_c \rho_c g)(k - k_{ws}) > 0 \Rightarrow \mathrm{Q}_2 \quad (1a)$$

$$< 0 \Rightarrow \mathrm{Q}_4 \quad (1b)$$

where g is the acceleration due to gravity, k is permeability, and h, ρ, v are symbols for enthalpy, density and kinematic viscosity. In two-phase conditions these quantities are indexed with (w) or (s) to denote the liquid or vapour phase, respectively; and note that at the critical point (c) the phases become identical. We have also $\gamma = K(\mathrm{d}T_{\mathrm{sat}}/\mathrm{d}P)$ and k_{ws} is the watershed 'permeability'

$$k_{ws} = \frac{J_M v_c \gamma_c}{J_E - h_c J_M + \gamma_c \rho_c g} = \frac{0.45066 \times K J_M}{J_E - 2.1074 \times 10^6 \times J_M + 0.01142 \times K} \times 10^{-12}\ \mathrm{m}^2 \quad (2)$$

using SI units. Assuming $J_M < 0$ we can distinguish two cases for the steady-state enthalpy $h \equiv |J_E/J_M|$: if

$$h < h_c - \gamma_c \rho_c g/(-J_M) \Leftrightarrow k_{ws} < 0 \quad (3a)$$

then all trajectories must leave C_- through the liquid boundary B_w, Case (1a). This corresponds to the low enthalpy class (23*a) for no conduction. However if

$$h > h_c - \gamma_c \rho_c \boldsymbol{g}/(-J_M) \Leftrightarrow k_{ws} > 0 \quad (3b)$$

then either Case (1a) or (1b) may hold. This corresponds to the intermediate/high enthalpy class (23*b) and (23*c).

When $k_{ws} > 0$ we can make the further classification (see Fig. 1*):

(1) If $k < k_{ws}$ then the trajectories must exit the physical region C_- of the flowplane through the liquid boundary B_w. The terminal state of these trajectories is single-phase liquid.
(2) If $k > k_{ws}$ then the trajectories leave C_- either
   (a) through the vapour boundary B_s, in which case the terminal state is single-phase vapour; or
   (b) through the stability boundary Γ. By analogy with the arguments presented in [1] we expect these trajectories to be conditionally stable when extended: when stable there is a jump to single-phase vapour at Γ. Stability here refers to the stability of the time-dependent equations (see [1]) when subject to a perturbation from the steady-state. Conditional stability means that the system may be numerically stable for some perturbations but not for others. Typically numerical instability has a cyclic character, with an amplitude which is dependent on the perturbation [1].

The two cases may be distinguished by computing, as before [1], the permeability label for the pressure trajectory which passes through the dry point S(0, −1)

$$k = \frac{J_M v_s \gamma}{J_E - h_s J_M + \rho_s g \gamma} = k_{sb} \quad (4a)$$

$$-1 = \frac{v_s}{k g \Delta h \Delta \rho}[J_E - h_w J_M + \rho_w g \gamma] - \frac{v_w v_s J_M \gamma}{k^2 g \Delta h \Delta \rho}. \quad (4b)$$

Equation (4a) is an expression for vapour boundary permeability k_{sb} (P; J_E, J_M, K) in terms of pressure, which is substituted into (4b) to give the dry-point pressure $P_d(J_M, J_E, K)$ and then the drypoint permeability $k_d(J_M, J_E, K)$. For small permeabilities $k < k_d$ Case (2a) follows (stable, single-phase vapour), while for large permeabilities $k > k_d$ Case (2b) is implied (conditionally stable).

3.2. *A high enthalpy reservoir*

Figure 2(i) shows the flowplane pressure trajectories for the reservoir parameters $J_M = -10^{-6}$ kgs^{-1} m^{-2}, $J_E = -2.9$ W m^{-2}, and $K = 4$ W m^{-1} K^{-1}. Here $h = |J_E/J_M|$ satisfies (3b). These are the same parameters used in the simulation example presented earlier (Fig. 1). They are similar to values used by Straus and Schubert [3] in their model of the vapour-dominated Kawah Kamojang geothermal system.

In Fig. 2(i) the trajectories are of two types, corresponding to permeabilities less than, or greater than, the watershed permeability, which in this case is computed from equation (2) to be $k_{ws} = 0.002156$ md. The trajectories should be compared with the corresponding curves for purely convective flow, Figs 4*(i) and (ii). The high pressure end of the trajectories in Fig. 2(i) $k < k_{ws}$ ($k > k_{ws}$) is qualitatively similar to the non-conductive cases (Figs. 4*(i) and (ii)), while the effect of conduction is apparent at the low pressure/temperature end: Fig. 2(i) may be derived (qualitatively) from Figs 4*(i) and (ii) by bending the low pressure end of the trajectories up and around until they meet the w-axis. Fig. 2(i) bears the same relationship to Figs 4*(i) and (ii) as does the conductive heatpipe (Fig. 2*(ii)) to the purely convective one (Fig. 2*(i)).

For low permeabilities in Fig. 2(i) there is a cut-off value $k_{\min}$ (determined from the solution of $s(P,k) = 0 = \partial s/\partial P$) below which ($k < k_{\min}$) there can be no two-phase zone, and for permeabilities near to (but greater than) $k_{\min}$ conditions are entirely liquid-domi-

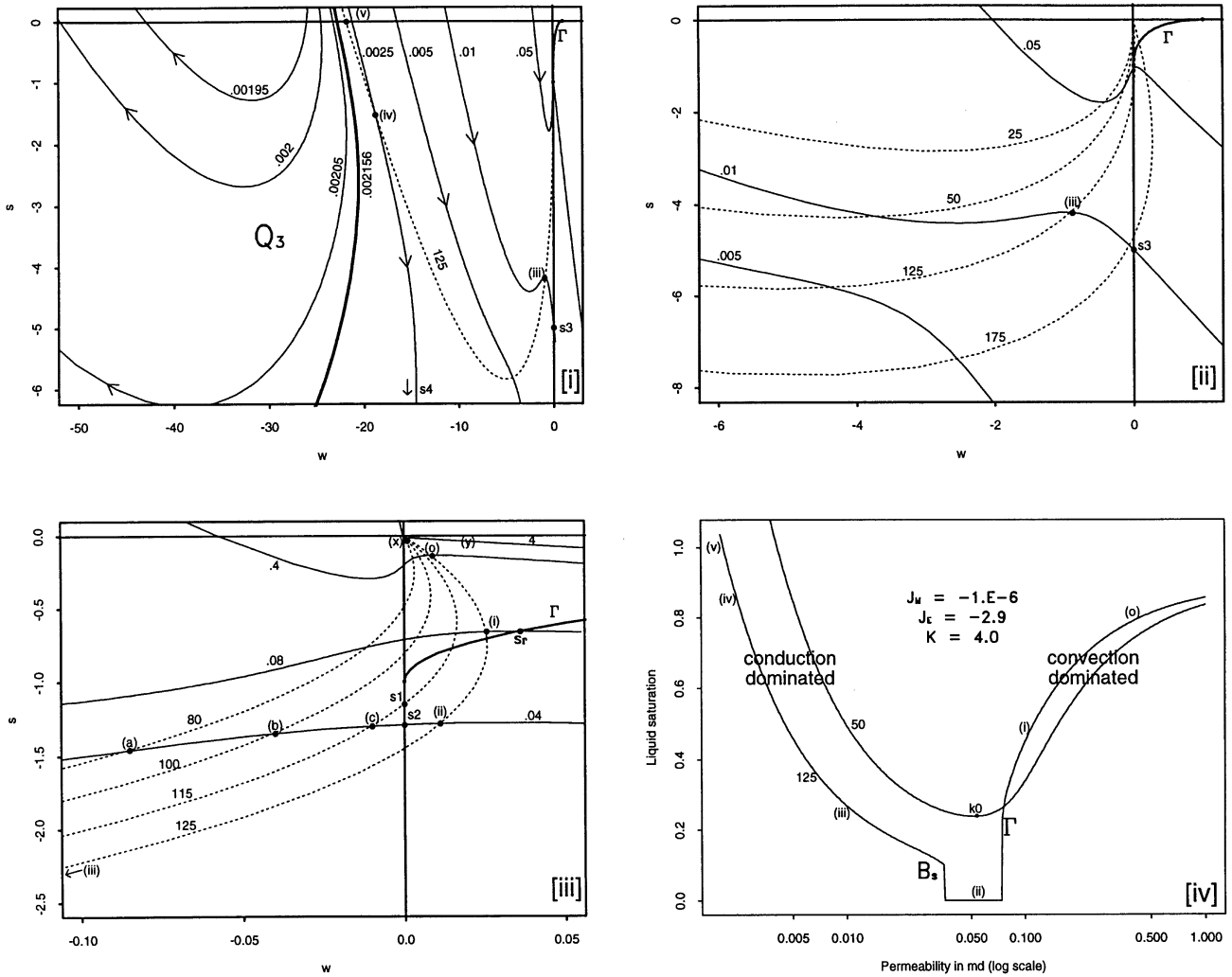

Fig. 2. Flowplane diagrams for the high enthalpy example ($J_M = -10^{-6}$ kg s^{-1} m^{-2}, $J_E = -2.9$ W m^{-2}, and $K = 4$ W m^{-1} K^{-1}). (i) Pressure trajectories (solid lines) labelled in millidarcies. Pressures increase in the direction of the arrows. The thick solid line is the pressure trajectory for the watershed permeability, equation (2). The dotted line is the $P = 125$ bar pressure contour. (ii) An enlargement of part of Fig. 2(i) showing pressure trajectories (solid lines) labelled in millidarcies, and pressure contours (dotted lines) labelled in bars. (iii) An enlargement of part of Fig. 2(ii). Bracketed symbols are explained in the text. (iv) Saturation/permeability curves at pressures of 50, 100, and 125 bars. $k_0(P)$ is the permeability corresponding to the minimum saturation on each curve; (0)...(v) on the $P = 125$ bar curve are referred to in the text, and correspond to points in Figs 2(i)–(iii); Γ and B_s correspond to parts of the flowplane boundary.

nated. This is a conductive effect (it cannot occur for purely convective flow).

Figures 2(ii) and (iii) show magnified portions of Fig. 2(i) nearer the flowplane origin. The pressure trajectories (solid lines) leave C_- either through the vapour boundary B_s or the stability boundary Γ. For this example the drypoint permeability is computed form equation (3) to be $k_d = 0.0536$ md (and drypoint pressure $P_d = 108.98$ bars). For $k > k_d$ the two phase zone terminates at the liquid residual saturation; below this is single-phase vapour. For $k < k_d$ the model is either unstable when extended downwards, or the two-phase zone terminates at the stability boundary at a pressure P_Γ and saturation S_Γ computed from equations (12*) and (13*); below this is single-phase vapour. For still greater permeabilities the trajectory is confined entirely to $\Delta \subset Q_4$ corresponding to the high enthalpy class (23*c) defined in Part 1. The relevant permeability limit is computed from equation (9*) with $s = 0 = w$, and in the present example has the value $k = 8.01$ md. For permeabilities greater than this the pressure trajectories are qualitatively similar to those of Fig. 2*(ii) in [1].

Also shown in Figs 2(ii) and (iii) are some pressure contours (dotted lines). Comparing with Fig. 4*, all the contours still emanate from the origin, but they are no longer straight lines. This is because the interaction term i in equation (9*) is now non-zero. The distorting effect of conduction bends these rays around to intersect the w-axis. Note that some of the pressure contours intersect the vapour boundary B_s. In Fig. 2(iii) the detail of the 4 md trajectory near the origin has the same general character as the 0.4 md trajectory. The close spacing of the pressure contours here implies that there is rapid pressure change along the trajectory very close to the flowplane origin. Thus the saturation along this trajectory is close to vapour residual except for very high pressures.

Permeability contrasts: fixed magnitude, varying depth. Now consider the effect of a rapid permeability change, e.g. an increase downward. We take as a typical trajectory the 0.04 md curve in Fig. 2(iii). At a given depth there is a rapid increase in permeability, and the flowstate moves along a dotted line pressure contour towards the origin. The diagram shows contours passing through (a), (b), (c) corresponding to permeability changes at pressures of 80, 100, 115 bars, respectively. In Fig. 2(iii) the pressure trajectories labelled $k = 0.04$, 4 md are the values (L), (H) used in the simulation, see Fig. 1.

The pressure of $P = 80$ bars is nearly that at the phase boundary near $z = 50$ m in Fig. 1. Thus the state trajectory implied by Fig. 1(i) enters the Fig. 2(iii) flowplane diagram at the intersection of the 80 bar contour with the 4 md pressure trajectory [near (x)]. It travels only a very short distance along this trajectory in the direction of (y). The state trajectories corresponding to Figs 1(ii)–(iv) all enter the flowplane at the intersection of the 80 bar contour with the 0.04 md pressure trajectory [at (a)]. Saturations here are close to liquid residual. The state for Fig. 1(ii) follows the 0.04 md trajectory to the point (b) on the 100 bar contour; here the state jumps along the pressure contour until it encounters the 4 md pressure curve near (x); as in Fig. 1(i) it then travels down this trajectory a short distance. The complete state trajectory is (abxy). Note that trajectories corresponding to Figs 1(i) and (ii) will eventually intersect the flowplane boundary Γ. They are numerically stable at 1200 m, but may not remain so at greater depths. If stability is maintained then the transition to single-phase vapour will occur close to the critical point at $P_\Gamma = 220.66$ bars and at the liquid saturation $S_\Gamma = 0.4785$ (computed from equations (9*) and (12*)).

The state trajectory for Fig. 1(iii) begins in the same way as for Fig. 1(ii). The permeability discontinuity is now somewhat deeper, at about 115 bars. However, the 115 bar pressure contour in Fig. 1(iii) differs in a vital way from the 100 bar contour, namely it crosses the s-axis below the dry point S(0, −1) and so exits from the flowplane at the point (s_1) on the vapour boundary B_s. This explains the fundamental difference in character between Fig. 1(ii) and Fig. 1(iii). The state trajectory for this example is (acs_1), followed by a single-phase vapour leg. The trajectory is always stable. For Fig. 1(iv) the permeability discontinuity is below the phase boundary so the path is (as_2) with a smooth transition to single-phase vapour at the liquid residual saturation (point s_2).

Permeability contrasts: fixed depth, varying magnitude. The effect on saturation of a rapid permeability change is summarized in Fig. 2(iv). The permeability $k_0(P)$ at the minimum of each $P = \text{const.}$ curve $S = S(k)$ is easily obtained from equations (9*) and (13*). For $k > k_0$ the liquid saturation increases with increasing permeability, while for $k < k_0$ the saturation decreases with increasing permeability. This is demonstrated by the 50 bar curve in Fig. 2(iv).

However, more complicated configurations are possible. Figure 3 shows a series of numerical simulations involving a permeability contrast at a fixed depth, but of varying magnitude. For convenience we have imposed a 50 bar pressure at the top of the model. The permeability contrast at 905 m depth then has an associated pressure of approximately 125 bars. This time we consider a permeability decrease. Figures 3(i)–(v) show the character of the response is highly dependent on the magnitude of the decrease.

The saturation profile above the permeability contrast is represented by the $k = 0.4$ md pressure trajectory shown in Fig. 2(iii). The effect of the permeability decrease is represented by motion along the 125 bar contour which is shown as a dotted line in Figs 2(i)–(iii), see also Fig. 2(iv).

For a decrease in permeability from 0.4 to 0.08 md and the motion is from (0) to (i) in Fig. 2(iii), and the saturation decreases accordingly. After this the 0.08 md

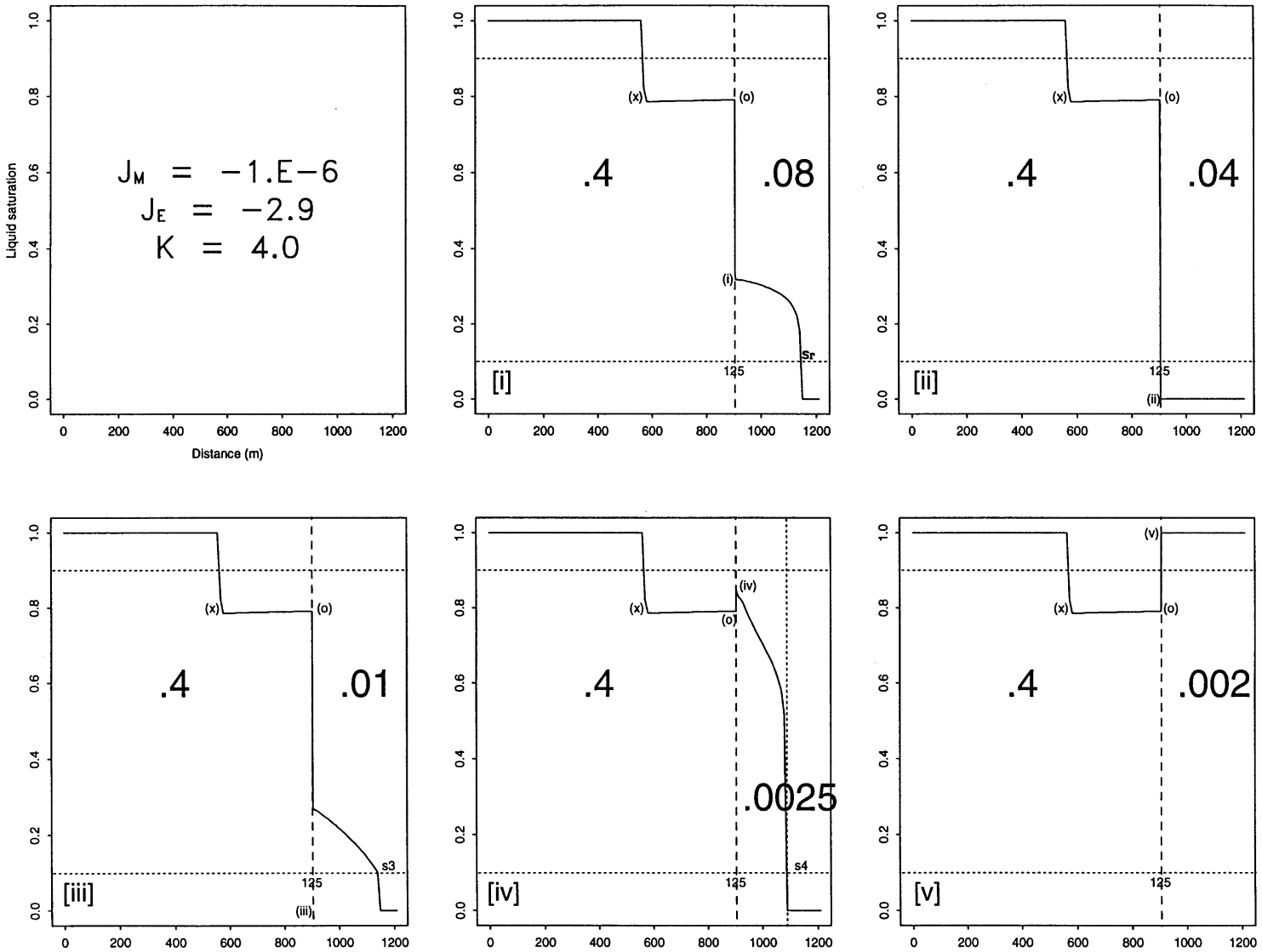

Fig. 3. Simulated saturation profiles including a permeability contrast (a decrease) at fixed depth (vertical dashed line) but of varying magnitude. The vertical dotted line in Fig. 3(iv) indicates the location of the critical point.

pressure trajectory is followed until it intersects the stability boundary at about $S_\Gamma = 0.25$, $P_\Gamma = 134$ bars. This is in agreement with Fig. 3(i) which shows a stable transition to single-phase vapour at about this pressure and saturation. This $C = 0$ transition is similar to the heatpipe example in Fig. 3*(i) of [1].

For a permeability decrease to 0.04 md the flowstate is translated to the point (ii) on the $P = 125$ bar contour (Fig. 2(iii)). Since this lies off the flowplane in the fourth quadrant, the only possible transition is to single-phase vapour (Fig. 3(ii)). However, if the permeability is decreased still further, to 0.01 md corresponding to Fig. 3(iii), the contour is followed back onto the third quadrant of the flowplane, at (iii) in Figs 2(i)–(iii). The saturation now decreases with increasing permeability as is shown by the $P = 125$ bar line in Fig. 2(iv). After the permeability change the state trajectory follows the $k = 0.01$ md trajectory (shown in Figs 2(i) and (ii)) until it intersects the vapour boundary B_s. At this point (s_3) there is a smooth (TS) transition to single-phase vapour.

A permeability decrease from 0.4–0.0025 md produces the saturation profile shown in Fig. 3(iv). The corresponding state trajectory passes through the point (iv) in Fig. 2(i). This induces a saturation increase across the discontinuity relative to the initial value (0), see Fig. 2(iv). After the permeability change the $k = 0.0025$ md pressure trajectory is followed (towards s_4) with a very rapid change in saturation for high pressures (near the critical value). This becomes more pronounced as the watershed permeability $k_{ws} = 0.002156$ md is approached (Fig. 2(i)). Finally if the downside permeability is less than the liquid boundary value ($k_{wb}(P) = J_M v_w \gamma/(J_E - h_w J_M + \rho_w g\gamma) = 0.00233$ md in this case) then there is a jump to single-phase liquid conditions. This is shown in Fig. 2(i) for the $k = 0.002$ md trajectory passing through the point (v), and the corresponding numerical simulation is given in Fig. 3(v). Further complications arise if the pressure contour intersects the watershed trajectory (which in this case it will do for $P > 143.0156$ bars), but we leave this as an exercise to the reader.

The $P = 125$ bar curve in Fig. 2(iv) provides a summary of these permeability/saturation changes. The role of conduction (or more precisely the interaction function $i(P)$ defined in equation (9*)) is evident in the left branch of the k–S curves. For $k < k_0$ we can say that the two-phase flow is conduction-dominated, while for $k > k_0$ it is convection-dominated. Note that the $P = 125$ bar curve is not always reversible. In the simulation example Fig. 3 the direction was from right to left (high permeability to low). If however the motion is in the opposite direction, i.e. a permeability increase (corresponding to the example in Fig. 1), then the right branch of the curve is not accessible from the left. The reason for this is to be found in the different roles played by the stability boundary Γ and the vapour boundary B_s in the flowplane geometry. The latter is a true boundary to the flowplane : only single-phase states can exist on a trajectory which leaves C_ through B_s. In contrast Γ is not a true boundary, it merely separates the stable states (for our boundary conditions : on C_) from the unstable ones (on C_+). Thus, a trajectory which leaves C_ through Γ does not necessarily leave the flowplane, and Fig. 3(iii)–(v) provides numerical evidence of this.

4. Vapour-dominated reservoirs

Figure 1(iii), represented by the path (acs_1) in Fig. 2(iii), is our prototype of a vapour-dominated reservoir. The necessary conditions for its existence are that the caprock formation L must be sufficiently tight and sufficiently deep. More precisely, the caprock permeability k and the pressure P at the junction between the caprock and aquifer must satisfy

$$k < k_d, \quad P > P_d \tag{5}$$

where k_d, P_d are the drypoint permeability and pressure, respectively, see equation (3). The aquifer permeability is not constrained in this model since any permeability increase with depth will augment the vapour content of the reservoir (compare with Part I where a permeability increase always leads to an increase in the reservoir liquid content). For the path (acs_1) the permeability increase induces a jump to single-phase vapour, but a jump to drier two-phase conditions is also possible (see Fig. 2(iv)).

Ingebritsen and Sorey [4] have used a series of numerical experiments to study the formation of vapour-dominated zones in geothermal reservoirs. Their simulation models are all two-dimensional, so direct comparison with the present theory is not possible. Our interest is in trying to determine which aspects of the two-dimensional simulations can be related to (are explained by) the one-dimensional theory, and which are essentially new phenomena.

Figure 4(i) shows pressure and saturation profiles for one of Ingebritsen and Sorey's examples. The aquifer permeability is $k_h = 100$ md and the caprock permeability is $k_l(2) = 0.05$ md. The selection of a suitable (J_E, J_M, K) is somewhat arbitrary. A mass flow of 2 kg s^{-1} of 310°C liquid is injected at the base of the model, and there is in addition a conductive energy flux of around 1.53 W m^{-2} which enters the reservoir through this boundary. However the mass flow through the base is not uniformly distributed, and there are additional lateral mass and energy flows which enter or leave the central reservoir at depth. In order to fix the equivalent one-dimensional fluxes we have therefore chosen the mass and energy values at the top of the vapour-dominated zone. For an area of 6 km^2 the mass flux is taken as $J_M = -0.67 \times 10^{-6}$ kg s^{-1} m^{-2} and the energy flux is about $J_E = -2.14$ W m^{-2}. Conductivity is $K = 1.67$ W m^{-1} K^{-1}.

Figure 4(ii) shows flowplane pressure trajectories and contours for this example corresponding to the pressure

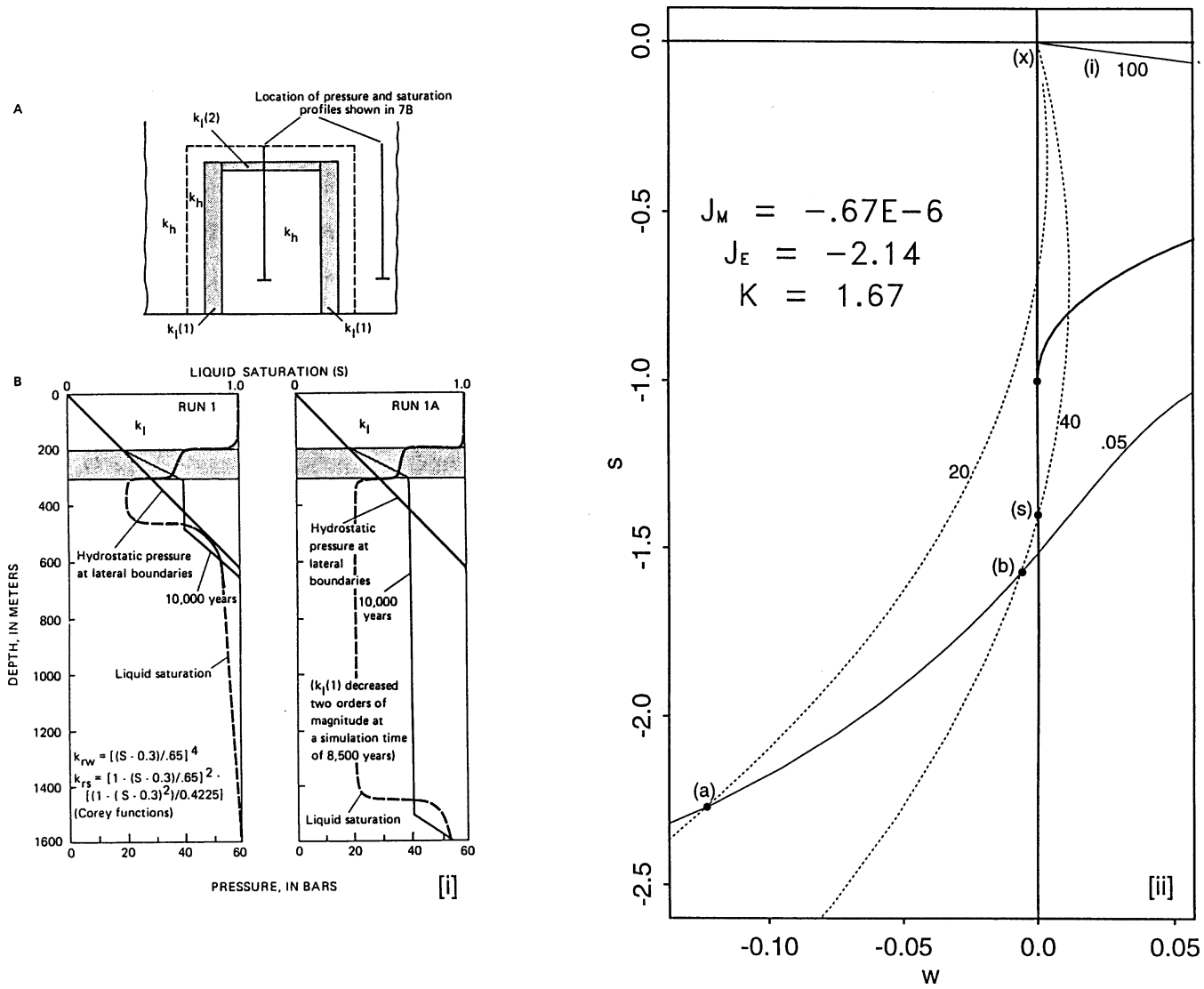

Fig. 4. (i) Reproduced from Ingebritsen and Sorey [4]. Part A defines $k_l(1)$ and $k_l(2)$ and shows the location of the pressure and saturation profiles in part B. (ii) The flow diagram appropriate to a one-dimensional approximation of the two-dimensional simulation example [4]. The state trajectory (xabs) matches aspects of the saturation and pressure profiles in Fig. 4(i).

and saturation profiles given in Fig. 4(i). The following sequence demonstrates the correspondence:

(1) Two-phase conditions first develop above the caprock structure at 200 m, point (x) on the 100 md pressure trajectory in Fig. 4(ii).
(2) then there is a rapid decrease in saturation at the upper boundary of the caprock. This occurs at abut 20 bars in Fig. 4(i), so the flowplane representation of the permeability discontinuity is the segment (xa) of the 20 bar pressure contour in Fig. 4(ii).
(3) After this there is a further decline in saturation through the caprock structure, see Fig. 4(i), until the lower caprock boundary is encountered at about 40 bars. In the flowplane (Fig. 4(ii)) this is represented by the segment (ab) of the 0.05 md pressure trajectory.
(4) At the lower boundary there is a further step decrease in saturation (Fig. 4(i)). The flow-plane represents this as the segment (bs) of the 40 bar pressure contour. The final state (s) in Fig. 4(ii) is single-phase vapour.

The flowplane picture based on one-dimensional theory is thus in broad qualitative agreement with the simulated pressure and saturation profiles derived from the two-dimensional numerical model. In particular, the numerical model (Fig. 4(i)) shows a step saturation decrease for both a permeability decrease (at the top of the caprock layer) and a permeability increase (at the bottom of the caprock layer). This would be difficult to explain without the understanding provided by the flowplane theory.

However there is no dry-out to single-phase vapour in the simulation Fig. 4(i) (although the saturation is close to liquid residual $S_{rw} = 0.3$), and conditions are liquid-dominated at depth. This is partly because of lateral inflow which produces wetter conditions at depth. Run 1A in Fig. 4(i) demonstrates that if the lateral permeability $k_l(1)$ is reduced then the vapour-dominated zone extends towards the base of the model (Ingebritsen and Sorey state that if the lateral barriers were completely impermeable, then the vapour-dominated zone "would tend to keep growing indefinitely"). Another factor may be that the simulations have been halted at 10 000 years and have not been run to steady-state. We have found that one-dimensional simulations on a similar scale require 30 000 years or more to reach steady-state, and the dry-out to single-phase vapour occurred towards the end. Thus it is conceivable that dry-out may actually take place with a longer simulation time. A third factor may be that Ingebritsen and Sorey's simulations used Corey relative permeabilities which do not satisfy the normality condition equation (1*) assumed (for convenience) in this paper.

Ingebritsen and Sorey suggest criteria for the development of a vapour-dominated zone, based on their simulation examples: the requirements are that the caprock permeability should be sufficiently low (less than 0.1 md), and that the aquifer permeability should be sufficiently high (greater than 1 md). Our results for one-dimensional systems show that the caprock permeability must satisfy $k < k_d$, where the dry-point permeability k_d is defined in terms of the steady-state parameters J_E, J_M and the conductivity K. For the parameters chosen we find $k_d \approx 0.1$ md, identical with Ingebritsen and Sorey's value. In addition, however, we require that the pressure at the caprock/aquifer interface satisfy $P > P_d$ where P_d (≈ 29 bars) is the dry-point pressure: hence the caprock structure must be sufficiently deep to permit vapour to persist at depth. Ingebritsen and Sorey do not identify this as a major factor in their study. Conversely, the value of the aquifer permeability does not appear to be an important factor in our work.

Ingebritsen and Sorey have noted the importance of conductive heatflow in their examples. Only when the ratio of conductive to convective heat input is sufficiently large (about 12:1 in their study) will vapour-dominated conditions develop. This places an upper limit on the mass flow (about 2 kg s^{-1}). In our one-dimensional theory we have also emphasized the vital importance of conduction for the formation of vapour-dominated reservoirs. Ingebritsen and Sorey's condition appears to be similar to our requirement that the reservoir be of high enthalpy type, equation (4a): if the mass flow in this equation refers to a fixed enthalpy fluid at the base of the reservoir then the excess energy must be transported conductively. Ignoring the gravitational term in equation (4a) we find that this equation implies $-J_M < -J_{EK}/(h_c - h_w)$, where J_{EK} is the conductive energy flow and h_w is the enthalpy of the (liquid) inflow. For Ingebritsen and Sorey's examples $J_{EK} \approx 10$ MW and $h_w = 1.4$ MJ kg^{-1}. Hence we need $|J_M| < 14$ kg s^{-1} for the reservoir to be of high enthalpy type. For $|J_M|$ near 14 kg s^{-1} we will get a very limited range of vapour-dominated state trajectories. As $|J_M|$ decreases this range will expand. Ingebritsen and Sorey's value of 2 kg s^{-1} is specific to the examples in their paper.

Ingebritsen and Sorey's paper also gives examples of vapour-dominated conditions which evolve for zero mass inflow. In one-dimension we have shown that if the net mass flux is zero (a heat-pipe) and geothermal boundary conditions operate, then the state trajectory cannot represent a vapour-dominated reservoir with a caprock. However there is no contradiction here because the net mass flux in Ingebritsen and Sorey's example will be non-zero in the vapour-dominated region (there will be a net mass upflow). Hence the example is not a heatpipe in the formal sense.

Overall there appear to be many points of agreement between Ingebritsen and Sorey's two-dimensional simulations and the present one-dimensional theory. Further work is needed to make the connection more precise. In particular it would be worth looking for vapour-domi-

nated zones in multi-dimensional models which suddenly disappear when the caprock permeability is increased beyond a certain value, or when the caprock is moved upwards past a certain minimum depth. We also recommend that all such models be extended vertically until single-phase conditions are encountered at depth. If instabilities are encountered in the steady-state simulations this fact should be noted.

5. Summary and conclusions

In this paper we have described a method for the study of one-dimensional (vertical) steady-state geothermal flows. The method is primarily graphical and leads to a general characterization of all such flows, subject to the restrictions set out in the Introduction to Part I [1]. In particular it is always assumed that pressure (and usually temperature) control are maintained at ground surface (geothermal boundary conditions), and that the system is 'bottom-heated'.

Our results show that there is a natural division of one-dimensional two-phase geothermal models into 'low enthalpy' and 'high enthalpy' types based on the steady-state values of mass and energy flow, and on conductivity. Low enthalpy systems have the property that they can only terminate in single-phase liquid at depth. High enthalpy systems can terminate in either single-phase liquid (for low permeabilities), or they may be unstable (for high permeabilities), or they may terminate in single-phase vapour (for high and intermediate permeabilities).

A suggested prototype of a vapour-dominated reservoir involves a permeability increase (caprock over aquifer). The necessary conditions are that the system is of high enthalpy type, and that the caprock is both sufficiently tight and sufficiently deep. Vapour-dominated models of this kind always terminate in single-phase vapour.

The role of conduction is seen to be essential for the formation of the vapour-dominated reservoir. More generally we have shown that, in the absence of conduction, a permeability increase (with depth) acts to increase the liquid saturation. The same conclusion holds for a heat-pipe (zero net mass flow) with conduction. Only for a non-zero net mass flow combined with conduction is it possible for a permeability increase to give rise to a decrease in liquid saturation. It is this kind of behaviour which permits the construction of the prototype vapour-dominated reservoir model.

The theory also shows that reservoir models (and presumably real-world reservoirs) can respond in a non-uniform manner to changes in their parameters. In fact an infinitesimal change to certain critical parameters can bring about a dramatic global change in the reservoir, e.g. a change from liquid-dominated to vapour-dominated conditions.

We have shown the utility of the flowplane diagram in the study of one-dimensional steady-state two-phase hydrothermal flows in a heterogeneous porous medium. The connection between permeability and saturation has not been clear in the past, and some errors of fact have arisen. Hopefully, by examining this problem in its natural context, that of the flowplane, some of the confusion surrounding it will be dispelled.

In this paper the flowplane is labelled by the steady-state mass and energy flow (and by the conductivity). These are also the quantities which are constant in the natural state of a geothermal field. Thus the flowplane diagram may become a useful tool for the reservoir engineer in profiling the field in its natural state. Some aspects of multi-dimensional vapour-dominated reservoir simulations may be usefully described in terms of the present theory.

Acknowledgement

Thanks to Steve Ingebritsen for permission to use Fig. 4(i) (Fig. 7 from [4]) in this paper.

References

[1] Young RM. Classification of one-dimensional steady-state geothermal flows including permeability variations—I. Theory and special cases. Int J Heat Mass Transfer 1998;41:3919–35.
[2] White DE, Muffler JP, Truesdell AH. Vapour-dominated hydrothermal systems compared with hot-water systems. Econ Geology 1971;66:75–97.
[3] Straus JM, Schubert G. One-dimensional model of vapour-dominated geothermal systems. J Geophys Res 1981;86(B10):9433–8.
[4] Ingebritsen SE, Sorey ML. Vapour-dominated zones within hydrothermal systems : evolution and natural state. J Geophys Res 1988;93(B11):13 635–55.
[5] McGuiness M, Young R. 1-D geothermal models—the good, the bad, the unlikely. Proc 16th N.Z. Geothermal Workshop. Auckland University, 1994. pp. 21–7.
[6] Young RM. Phase transitions in one-dimensional steady-state hydrothermal flows. J Geophys Res 1996;101(B8):18 011–22.
[7] Pruess K. TOUGH2—a general-purpose numerical simulator for multiphase fluid and heat flow. LBL-29400, May, 1991.
[8] Sheu JP, Torrance KE, Turcotte DL. An experimental study of two-phase convection in a porous medium with applications to geological problems. J Geophys Res 1977;82:2045–53.
[9] Reda DC, Eaton RR. Influence of steam/water relative permeability models on predicted geothermal reservoir performance : a sensitivity study. Paper presented to the Sixth Annual Workshop on Geothermal Reservoir Engineering, Stanford University, 16–18 December 1980.
[10] Kissling W, McGuiness M, Weir G, White S, Young R. Vertical two-phase flow in porous media. Transport in Porous Media 1992;8:99–131.